



Coupled Thermodynamic Analysis on the Fire Response and Improvement of Fire Resistance of Steel Buildings

Jingbo An*, Chunhong Wang

Academy of City Construction and Transportation, Hefei University, Hefei 230601, China

Corresponding Author Email: ajbwch@hfuu.edu.cn

<https://doi.org/10.18280/ijht.400115>

Received: 28 September 2021

Accepted: 25 December 2021

Keywords:

steel buildings, fire response, coupled thermodynamic analysis, fire resistance

ABSTRACT

The poor fire resistance of steel buildings threatens structural security, and severely limits the application of such buildings in many countries. The existing studies have not carried out whole-process analysis on the temperature field distribution and deformation law of steel building components under fire. To solve the problem, this paper performs coupled thermodynamic analysis on the fire response of steel buildings, and tries to improve their fire resistance. Firstly, the dynamical properties of steel buildings in response to fire were analyzed, and a coupled thermodynamic model was constructed for these buildings. Next, the whole process of thermodynamic coupling was investigated for the fire response of steel buildings. Through experiments, the authors obtained the results of coupled thermodynamic analysis, and presented suggestions on how to improve fire resistance.

1. INTRODUCTION

Because of their lightweight, fast construction, good quality, and low cost, steel structures have gained more and more popularity in the construction industry [1-7]. Despite being prepared from non-combustible materials, steel structures witness a sharp decline of strength and stiffness in a hot environment [8-12]. The poor fire resistance of steel buildings threatens structural security, and severely limits the application of such buildings in many countries. The high temperature of fire brings several damages to the entire steel structure, and even causes the structure to collapse [13-18]. Fire zones and smoke zones can be set up in buildings to curb the combustion of inflammables, and slow down the diffusion of smoke. But these measures do not apply to all types of buildings [19-23]. Therefore, it is necessary to analyze the fire resistance, fire response, and post-fire safety of steel buildings.

Weisheim et al. [24] tested and numerically analyzed the fire resistance of the aqueous expansion coating on structural steel under natural fire. Based on a small-scale lab test, they developed an advanced numerical model to simulate the fire resistance of the coating under any fire scenario. Supported by the New Research Fund for Coal and Steel (RFCS), Alam et al. [25] conducted three large compartment natural fire tests in Ulster University, in an attempt to characterize the traveling fires between large compartments. The details on the second fire test were provided. In the second fire test, the opening size was reduced to generate a different ventilation condition from that of the first test. The results show that, regardless of the ventilation condition, the traveling fire always creates uneven temperatures within the compartments. The unevenness is related to the size of the opening. Hou et al. [26] summarized the test data on the high-temperature dynamical performance of steel strands, and established a regression model for the high-temperature performance of the steel strands, which applies to both theoretical analysis and numerical calculation.

Based on the non-steady temperature field model of high-rise large space building fires, the nonlinear finite-element analysis with the time integral effect was adopted to model the fire resistance of large-span prestressed steel structures. Manco et al. [27] reported the results of a numerical survey, aimed at assessing the structural safety of the upper components of real offshore steel structures exposed to unexpected local fires. Two different fire methods were adopted to acquire the nonlinear thermal stress and ultimate strength. The relevant results ensure the reliability of fire safety analysis, and prevent the main security (bearing) functions of offshore steel structures from being damaged under unexpected fires. Suwondo et al. [28] analyzed the robustness of a three-dimensional (3D) multilayered composite steel structures in multiple fire scenarios. Following the finite-element method, their analysis model was verified against the literature. Then, the anti-collapse property of the structures was modeled under various fire scenarios.

So far, the domestic and foreign research on the fire response of steel buildings concentrates on steel buildings with a limited space, and complete the fire resistance analysis of steel structures, in the light of load distribution and fire response time. However, the relevant scholars have not carried out whole-process analysis on the temperature field distribution and deformation law of steel building components under fire.

To solve the problem, this paper performs coupled thermodynamic analysis on the fire response of steel buildings, in a bid to improve their fire resistance. Section 2 analyzes the dynamical properties of steel buildings in response to fire, and constructs a coupled thermodynamic model for these buildings. Section 3 investigates the whole process of thermodynamic coupling for the fire response of steel buildings. Through experiments, the authors obtained the results of coupled thermodynamic analysis, and presented suggestions on how to improve fire resistance.

2. DYNAMICAL ANALYSIS

Figure 1 illustrates the fire response in the space of a steel building. The basic idea of fire response is to divide the indoor space of the steel building into two parts: a hot smoke layer, and a cold air layer. The gas in each layer remains uniform in space. With the rising temperature of the fire, the yield strength and ultimate strength of the steel building gradually fall. When the fire temperature is greater than 300°C, the steel building loses all its yield strength and ultimate strength. When the temperature reaches 200–380°C, the toughness and plasticity of the building will be reduced by the blue brittleness. Once the temperature surpasses 400°C, the strength of the steel building will nosedive. By the time the temperature rises above 580°C, the steel building will be no longer carry any load.

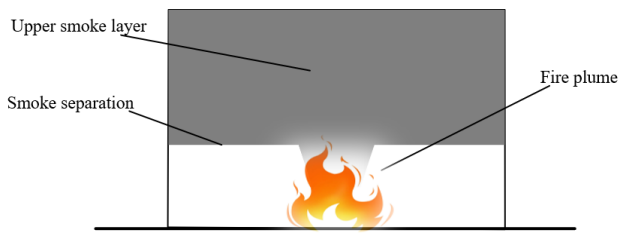


Figure 1. Fire response in the space of a steel building

Let g_b and g_{bp} be the yield strength at normal temperature and nominal yield strength at fire temperature of the steel building, respectively; g_{bp}/g_b be the reduction coefficient of nominal yield strength of the steel building at the fire temperature P_r . Then, the nominal yield strength of the steel building in response to fire can be calculated by:

$$g_{bp}/g_b = 1 + \frac{P_r}{770 \ln \frac{P_r}{1690}}, \quad 0^\circ C \leq P_r < 580^\circ C \quad (1)$$

$$g_{bp}/g_b = \frac{111 \left(1 - \frac{P_r}{1000}\right)}{P_r - 450}, \quad 580^\circ C \leq P_r < 1000^\circ C \quad (2)$$

According to the steel building design code of Australia, the nominal yield strength of the steel building in response to fire is defined as:

$$g_{bp}/g_b = 1.0, \quad 0^\circ C \leq P_r < 200^\circ C \quad (3)$$

$$g_{bp}/g_b = (880 - P_r)/700, \quad 200^\circ C < P_r \leq 880^\circ C \quad (4)$$

A more concise definition is as follows:

$$g_{bp}/g_b = 1 - 5 \times 10^{-4} P_r - 9 \times 10^{-7} P_r^2 \quad (5)$$

The general comprehensive fire-resistance design codes for buildings in Asia define $g_{bp}/g_b = R_1 - R_2 P_r - R_3 P_r^2$, where R_1 , R_2 , and R_3 are the regression coefficients depending on the types of steel buildings.

Let MO be the elastic modulus at normal temperature; MO_p be the initial elastic modulus of the steel building at the fire temperature P_r . The initial elastic

modulus of the steel building in response to high fire temperature can be calculated by:

$$\begin{aligned} MO_p/MO &= -16.8 \times 10^{-12} P_r^4 + 12.2 \times 10^{-9} P_r^3 \\ &\quad - 36.4 \times 10^{-7} P_r^2 + 16.4 \times 10^{-5} P_r + 1 \end{aligned} \quad (6)$$

$0^\circ C \leq P_r \leq 580^\circ C$

$$\begin{aligned} MO_p/MO &= 8.66 \times 10^{-4} (800 - P_r), \\ 600^\circ C \leq P_r &\leq 800^\circ C \end{aligned} \quad (7)$$

According to the steel building design code of Australia, the initial elastic modulus of the steel building in response to fire is defined as:

$$\begin{aligned} MO_p/MO &= 1.0 + P_r / 2000 \ln \left(\frac{P_r}{1100} \right), \\ 0^\circ C < P_r &\leq 580^\circ C \end{aligned} \quad (8)$$

$$\begin{aligned} MO_p/MO &= (680 - 0.68 P_r) / (P_r - 54.7), \\ 580^\circ C < P_r &\leq 1000^\circ C \end{aligned} \quad (9)$$

A more concise definition is as follows:

$$\begin{aligned} MO_p/MO &= -9.98 \times 10^{-7} P_r^2 \\ &\quad - 1.97 \times 10^{-4} P_r + 1 \end{aligned} \quad (10)$$

After lowering the order of fire temperature, the initial elastic modulus can be calculated by:

$$\begin{aligned} MO_p/MO &= (7.5 P_r - 5200) / (5.9 P_r - 4850), \\ 0^\circ C < P_r &\leq 580^\circ C \end{aligned} \quad (11)$$

$$\begin{aligned} MO_p/MO &= (980 - P_r) / (5.9 P_r - 2660), \\ 580^\circ C < P_r &\leq 1000^\circ C \end{aligned} \quad (12)$$

The simplest coupled thermodynamic model for steel buildings in response of fire is the piecewise linear function, which provides the strain at each thermal stress control point of the steel building at a fire temperature. The slightly more complex model is the continuous smooth function. Compared with the piecewise linear function, the continuous smooth function is easy to converge, and close to the reality. Let β and m be the parameters fitted by the function curve; ξ be the total thermal stress; MO be the Young's modulus of the steel structure material. The thermodynamical coupling relationship of the steel building material near its yield point can be described by the Ramberg–Osgood relationship:

$$\eta = \frac{\xi}{MO} + \beta \left(\frac{\xi}{MO} \right)^m \quad (13)$$

If the steel building is made of ordinary steel structures, the following formulas can be directly adopted:

$$\eta_\xi = \frac{\xi}{MO} + 0.43 \times \frac{g_b}{MO} \times \left(\frac{\xi}{g_b} \right)^{50}, \quad 0^\circ C \leq P_r \leq 60^\circ C \quad (14)$$

$$\eta_{\xi} = \frac{\xi}{MO_p} + 0.01 \times \left(\frac{\xi}{g_{bp}} \right)^m, \quad 60^\circ C \leq P_r \leq 880^\circ C \quad (15)$$

Let $\eta_{tp} = g_{tp}/MO_p$ be the proportional limit strain; MO_{tp} and η_{bp} be the plastic modulus and yield strain of the steel building at the fire temperature P_r , respectively; Φ_p and η_{vp} be the shape function and limit strain of the curve at the fire temperature P_r , respectively; ξ_{0p} be the reference stress at the fire temperature P_r . Based on the proportional limit strain, yield strain, and ultimate strain, the coupled thermodynamic model can be constructed by:

$$\xi = MO_p \eta_{\xi}, \quad 0 \leq \eta_{\xi} \leq \eta_{tp} \quad (16)$$

$$\xi = \frac{(MO_p - MO_{tp})\eta}{1 + \left| \frac{(MO_p - MO_{tp})}{\xi_{0p}} \right|^{\Phi_p}} + MO_{tp}\eta, \quad \eta_{tp} \leq \eta_{\xi} \leq \eta_{bp} \quad (17)$$

$$\xi = g_{bp}, \quad \eta_{bp} \leq \eta_{\xi} \leq \eta_{vp} \quad (18)$$

Figure 2 shows the flow of dynamical analysis of the steel building in response to fire.

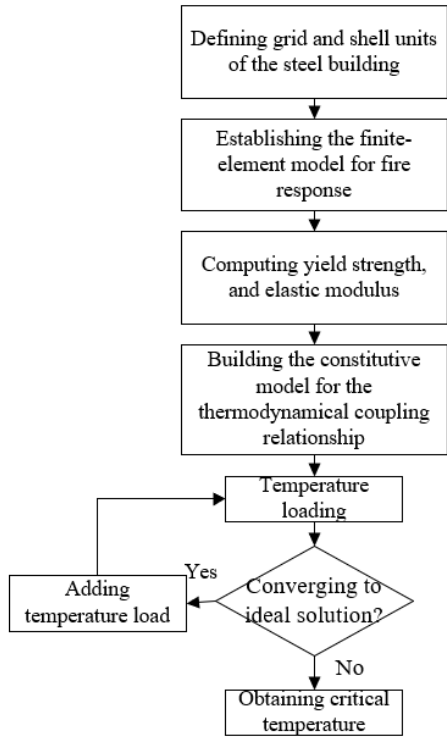


Figure 2. Flow of dynamical analysis of the steel building in response to fire

3. WHOLE-PROCESS THERMODYNAMIC COUPLING ANALYSIS

Based on the grid and shell structures, this paper carries out an instance analysis on the fire response of steel buildings. Figure 3 shows the analysis flow of the whole process of thermodynamic coupling for steel buildings. The entire process of fire was investigated with the aid of Matlab and finite-element analysis software.

The bars of steel buildings are relatively large. Thus, the compressive bars of steel structures are destabilized earlier than the strength failure of the bars of steel structures. Since the stability analysis related to slenderness ratio cannot be achieved based on the constitutive relationship of finite-element analysis, the critical load obtained by finite-element analysis is the critical load of the steel building under limit strength. Hence, the calculation result is reasonable for the tensile bars of the steel building, which adopts the ultimate strength and load limit in calculation. Meanwhile, the calculation result is exaggerated for compressive bars.

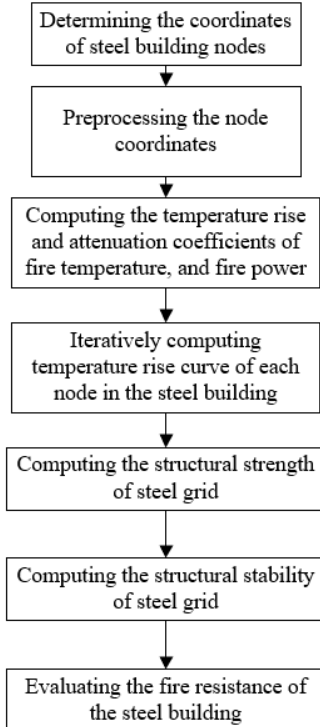


Figure 3. Analysis flow of the whole process of thermodynamic coupling for steel buildings

Let F_T be the axial tension or compression; S_m and S be the net and gross cross-sectional areas of the rod, respectively; g be the designed strength of the steel building under normal temperature; Ψ be the stability coefficient of the axial compressive bar under normal temperature. The strength of axial stressed bar of steel buildings under normal temperature can be calculated by:

$$\delta = \frac{F_T}{S_m} \leq g \quad (19)$$

Let χ_P be the strength reduction coefficient of the steel building under high temperature; ζ_S be the partial safety factor for resistance of the steel component. The strength of axial stressed bar of steel buildings under normal temperature can be calculated by:

$$\xi = \frac{F_T}{\Psi S} \leq g \quad (20)$$

The strength of axial tensile or compressive steel component of steel buildings responding to high fire temperature can be calculated by:

$$\frac{F_T}{S_m} \leq \chi_p \zeta_s g \quad (21)$$

Let Ψ_p be the stability coefficient of the axial compressive steel component in steel buildings responding to high fire temperature; β_d be the stability checking parameter. Then, the stability of axial compressive steel component in steel buildings responding to high fire temperature can be calculated by:

$$\frac{F_T}{\Psi_p S} \leq \chi_p \zeta_s g \quad (22)$$

$$\Psi_p = \beta_d \Psi \quad (23)$$

During finite-element preprocessing, the thermal stress-thermal strain curve of the axial compressive units in the steel building cannot be corrected, due to technical constraints. As a result, the stability coefficient Ψ_p cannot be introduced to the finite-element software, when the building is responding to high fire temperature. Under the premise of ensuring the stability of the steel building, the nonlinear finite-element solver of finite-element analysis cannot be fully utilized, unless the thermal stress of the compressive units of the building is extracted after each temperature loading, and imported to inequality (22) for comparison. If inequality (22) is satisfied, then the compressive bar of the steel structure can continue working; otherwise, the bar cannot work any longer, for it has reached the stability limit.

In the analysis system, the working unit corresponding to the compressive Bar is eliminated by the preset peripheral command. In the total stiffness matrix, the unit is replaced with zero. In this case, the overall stiffness of the steel structure will decline. If there are too many zero elements, the total stiffness matrix of the steel building will become a singular matrix. Then, the finite-element analysis will not converge. If a bar working unit connected to a node is removed from the steel structure, then the node could result in geometric variation. Neither will the finite-element analysis converge in this case. In other words, the steel building reaches the ultimate bearing capacity, and the critical temperature of the building is the fire temperature.

For simplicity, the least squares (LS) method is adopted to mathematically fit the cross-sectional stability coefficient ψ of various types of steel buildings. Let $\mu_m = \mu(g_b/MO)^{1/2}/\pi$ be the relative slenderness ratio of the component. If $\mu_m \leq 0.22$, then:

$$\Psi = 1 - \beta_1 \mu_m^2 \quad (24)$$

If $\mu_m > 0.22$, then:

$$\Psi = \left[\frac{(\beta_2 + \beta_3 \mu_m + \mu_m^2)}{\sqrt{(\beta_2 + \beta_3 \mu_m + \mu_m^2)^2 - 4\mu_m^2}} \right] / 2\mu_m^2 \quad (25)$$

4. EXPERIMENTS AND RESULTS ANALYSIS

Figures 4 and 5 present the temperature curves on the upper and lower chord nodes of the steel structure, respectively. The temperature of the upper chord nodes of the steel building peaked at around 700°C, about 100°C higher than the peak

temperature (600°C) of the lower chord nodes. Next, the authors computed the reduction coefficients for the yield strength, proportional limit strain, and initial elastic modulus of steel buildings under different fire temperatures (Table 1).

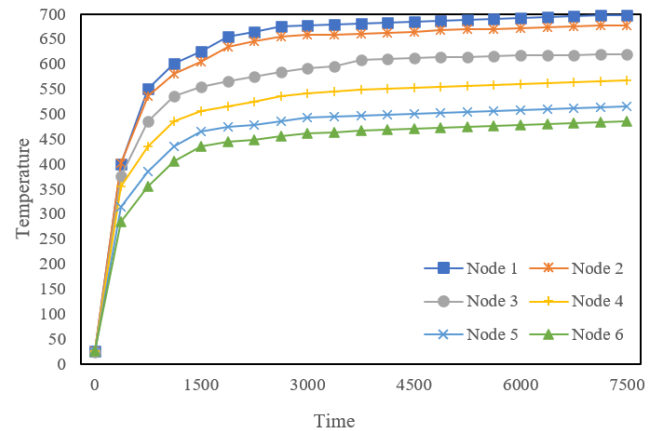


Figure 4. Temperature changes on the upper chord nodes of the steel structure

Table 1. Reduction coefficients of steel buildings

Temperature	Reduction coefficients		
	Yield strength	Proportional limit strain	Initial elastic modulus
50	1.307	1.117	1.6372
150	1.628	1.069	1.0628
250	1.485	0.482	1.4824
350	1.019	0.629	0.916
450	0.624	0.841	0.833
550	0.418	0.081	0.786
650	0.741	0.627	0.057
750	0.125	0.028	0.163
850	0.082	0.0462	0.0815
950	0.079	0.0397	0.0695

The steel structure in each stage was selected for internal force analysis, after removing compressive bars. Figure 6 shows how the axial tension varied with time. With the rise of temperature, the internal force of the bars in the steel building gradually increased, and ended up with stability failure. If the bar is a lower chord bar, the initial internal force is tension. As the temperature grows, the tension gradually turns into compression, and eventually leads to buckling failure. The lower chord bars carry fewer loads than the upper chord bars, because the temperature on lower chord bars increased slower than that on the upper chord bars.

As shown in Tables 2 and 3, under the effect of fire temperature, the deflection at different fire positions of steel buildings gradually increased, but the deformation degree and deformation rate differed between steel buildings. During the safety evaluation of steel buildings responding to fire, special focus should be laid on the beam body at the middle of the building. It is the place of the largest displacement, greatest deformation, and fastest deformation rate. The local failure probability of this place is greater than that in another other location.

Figures 7 and 8 compare the deflections and displacements at different fire positions, respectively. It can be seen that the fire position has largely the same effect on the entire steel building and its components: the constant rise of fire temperature causes continuous plastic deformation of the building, and eventually leads to fracturing.

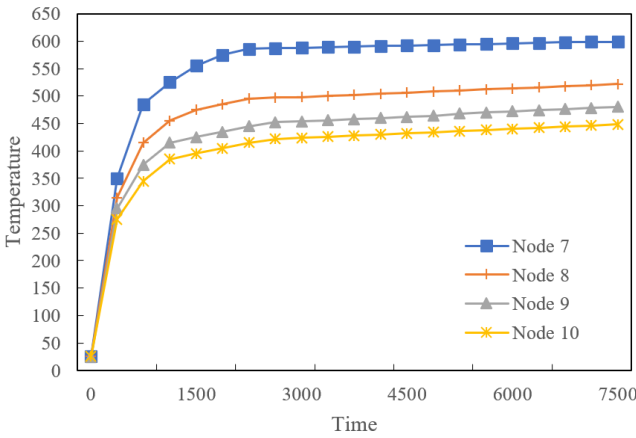


Figure 5. Temperature changes on the lower chord nodes of the steel structure

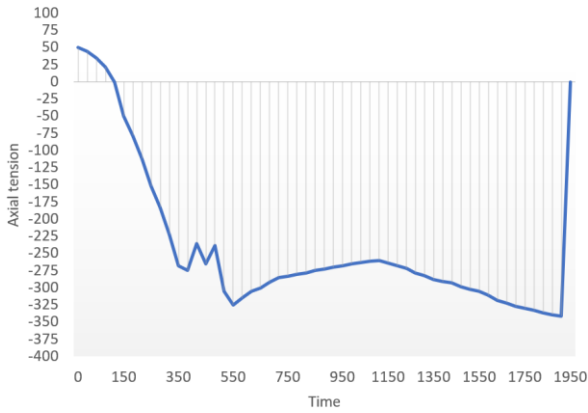


Figure 6. Axial tension-time curve of bars in the steel building

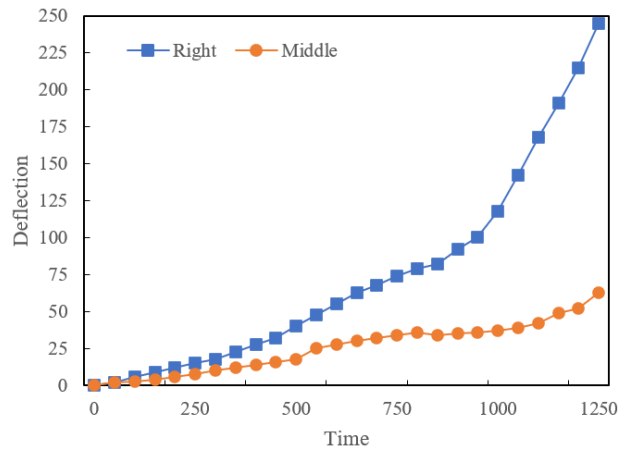


Figure 7. Deflections at different fire positions

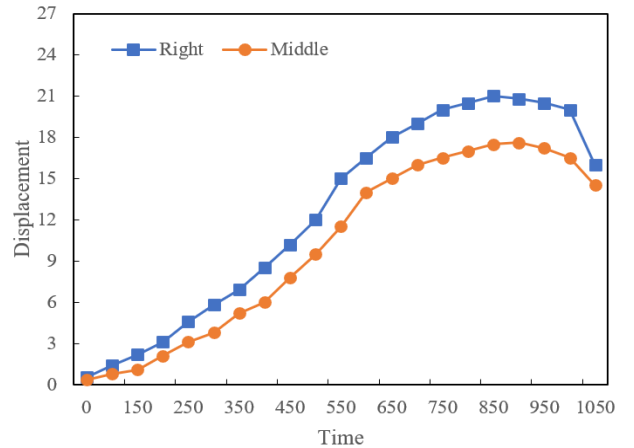


Figure 8. Displacements at different fire positions

Table 2. Deflection at different fire positions of steel buildings

Distance	50°C	150°C	250°C	350°C	450°C	550°C	650°C	750°C	850°C	950°C
2m	0.47	1.2	1.82	2.63	2.09	2.68	3.49	3.81	4.11	4.35
4m	1.75	1.63	6.37	3.47	7.18	9.37	11.75	13.84	14.12	114.85
6m	1.02	6.05	5.96	5.82	6.28	9.67	15.48	16.64	17.04	17.74
8m	2.48	4.05	5.09	7.22	7.14	8.48	9.68	10.46	11.54	12.25
10m	0.42	0.55	0.41	0.66	1.74	1.92	2.63	2.85	2.99	3.11

Table 3. Deformation rate at different fire positions of steel buildings

Distance	50°C	150°C	250°C	350°C	450°C	550°C	650°C	750°C	850°C	950°C
2m	0.04	0.08	0.04	0.29	0.19	0.47	0.48	0.62	0.68	0.74
4m	0.14	0.05	0.79	0.32	0.22	0.26	1.74	1.82	1.88	1.94
6m	0.32	0.16	0.36	0.67	0.43	0.96	1.82	1.94	1.99	2.04
8m	0.36	0.96	0.26	0.64	0.29	0.69	0.68	0.94	0.97	1.14
10m	0.29	0.25	0.61	0.83	0.16	0.14	0.22	0.27	0.30	0.36

5. CONCLUSIONS

This paper carries out coupled thermodynamic analysis on the fire response of steel buildings, with the goal of improving their fire resistance. Firstly, the authors analyzed the dynamical properties of steel buildings in response to fire, and built a coupled thermodynamic model for these buildings. On this basis, they analyzed the whole process of thermodynamic coupling for the fire response of steel buildings. Through experiments, the authors drew the temperature curves on the upper and lower chord nodes of the steel structure, and

computed the reduction coefficients for the yield strength, proportional limit strain, and initial elastic modulus of steel buildings under different fire temperatures. Furthermore, the steel structure in each stage was selected for internal force analysis, after removing compressive bars. The resulting axial tension-time curve of bars in the steel building confirm that: the lower chord bars carry fewer loads than the upper chord bars, because the temperature on lower chord bars increased slower than that on the upper chord bars. In addition, the deflections and displacements at different fire positions were compared. It was concluded that: During the safety evaluation

of steel buildings responding to fire, special focus should be laid on the beam body at the middle of the building. It is the place of the largest displacement, greatest deformation, and fastest deformation rate. The local failure probability of this place is greater than that in another other location.

REFERENCES

- [1] Mantič, M., Kuľka, J., Faltinová, E., Kopas, M. (2016). Autonomous online system for evaluating steel structure durability. *Diagnostyka*, 17(3): 15-20.
- [2] Jeon, S., Rigby, S.E. (2019). Design and numerical assessment of a rapid-construction corrugated steel-concrete-steel protective structure. *International Journal of Protective Structures*, 10(4): 470-485. <https://doi.org/10.1177/2041419619830703>
- [3] Shlyakhova, G.V., Barannikova, S.A., Bochkareva, A. V., Li, Y.V., Zuev, L.B. (2018). Structure of a carbon steel-stainless steel bimetal. *Steel in Translation*, 48(4): 219-223. <https://doi.org/10.3103/S0967091218040101>
- [4] Zajec, B., Bajt Leban, M., Kosec, T., Kuhar, V., Legat, A., Lenart, S., Karmen, F.B., Gavin, K. (2018). Corrosion monitoring of steel structure coating degradation. *Tehnički Vjesnik*, 25(5): 1348-1355. <https://doi.org/10.17559/TV-20170206004112>
- [5] Hou, Y., Li, Z., Ni, S., Gong, J. (2019). Structural responses of a modular thin-walled steel trestle structure. *Journal of Constructional Steel Research*, 158: 502-521. <https://doi.org/10.1016/j.jcsr.2019.03.013>
- [6] Li, Z., La, P., Ma, J., Guo, X., Sheng, J., Shi, Y., Zhou, X. (2019). Superior strength and ductility of 1045 steel with heterogeneous composite structure. *Materials Letters*, 238: 191-193. <https://doi.org/10.1016/j.matlet.2018.12.006>
- [7] Gundyrev, V.M., Zel'dovich, V.I., Schastlivtsev, V.M. (2016). Carbon distribution in the martensite structure of structural steel. In *Doklady Physics*, 61(5): 215-217. <https://doi.org/10.1134/S1028335816050013>
- [8] Koptseva, N.V., Efimova, Y., Nikitenko, O.A., Baryshnikov, M.P., Zherebtsov, M.S. (2016). Formation of ultrafine-grain structure in carbon steel by high-temperature high-speed compression. *Steel in Translation*, 46(2): 103-106. <https://doi.org/10.3103/S0967091216020066>
- [9] Stratulat, A., Duff, J.A., Marrow, T.J. (2014). Grain boundary structure and intergranular stress corrosion crack initiation in high temperature water of a thermally sensitised austenitic stainless steel, observed in situ. *Corrosion Science*, 85: 428-435. <https://doi.org/10.1016/j.corsci.2014.04.050>
- [10] Tong, M.W., Venkatsurya, P.K.C., Zhou, W.H., Misra, R.D.K., Guo, B., Zhang, K.G., Fan, W. (2014). Structure-mechanical property relationship in a high strength microalloyed steel with low yield ratio: The effect of tempering temperature. *Materials Science and Engineering: A*, 609: 209-216. <https://doi.org/10.1016/j.msea.2014.05.004>
- [11] Churymov, A.Y., Khomutov, M.G., Pozdnyakov, A.V., Mukhanov, E.L. (2014). Study of the structure and high-temperature mechanical properties of a steel with an elevated content of boron. *Metal Science and Heat Treatment*, 56(5): 336-338. <https://doi.org/10.1007/s11041-014-9757-2>
- [12] Craveiro, H.D., Rodrigues, J.P.C., Santiago, A., Laím, L. (2016). Review of the high temperature mechanical and thermal properties of the steels used in cold formed steel structures—The case of the S280 Gd+ Z steel. *Thin-Walled Structures*, 98: 154-168. <https://doi.org/10.1016/j.tws.2015.06.002>
- [13] Wang, J., Wang, G. (2014). Influences of montmorillonite on fire protection, water and corrosion resistance of waterborne intumescent fire retardant coating for steel structure. *Surface and Coatings Technology*, 239: 177-184. <https://doi.org/10.1016/j.surfcoat.2013.11.037>
- [14] Bilotta, A., de Silva, D., Nigro, E. (2016). Tests on intumescent paints for fire protection of existing steel structures. *Construction and Building Materials*, 121: 410-422. <https://doi.org/10.1016/j.conbuildmat.2016.05.144>
- [15] Mans, V., Lugato, L., Garcia, D. (2016). Ammonium polyphosphates and intumescent coatings in structural steel fire protection. *PPCJ Polymers Paint Colour*, 206(4620): 23-27.
- [16] Akaa, O.U., Abu, A., Spearpoint, M., Giovinazzi, S. (2016). A group-AHP decision analysis for the selection of applied fire protection to steel structures. *Fire Safety Journal*, 86: 95-105. <https://doi.org/10.1016/j.firesaf.2016.10.005>
- [17] Xue, Y., Zhang, S., Yang, W. (2015). Influence of expanded vermiculite on fire protection of intumescent fireproof coatings for steel structures. *Journal of Coatings Technology and Research*, 12(2): 357-364. <https://doi.org/10.1007/s11998-014-9626-3>
- [18] Mohammadi, S., Sharifpanahi, H., Taromi, F.A. (2015). Influence of hybrid functionalized graphite nanoplatelets-tripolyphosphate on improvement in fire protection of intumescent fire resistive coating for steel structures. *Polymer Degradation and Stability*, 120: 135-148. <https://doi.org/10.1016/j.polymdegradstab.2015.06.017>
- [19] Wang, G.J., Yang, J.Y. (2010). Influences of binder on fire protection and anticorrosion properties of intumescent fire resistive coating for steel structure. *Surface and Coatings Technology*, 204(8): 1186-1192. <https://doi.org/10.1016/j.surfcoat.2009.10.040>
- [20] Sadiq, H., Wong, M.B., Al-Mahaidi, R., Zhao, X.L. (2013). A novel active fire protection approach for structural steel members using NiTi shape memory alloy. *Smart Materials and Structures*, 22(2): 025033. <https://doi.org/10.1088/0964-1726/22/2/025033>
- [21] Ullah, S., Ahmad, F., Shariff, A.M., Bustam, M.A. (2014). Synergistic effects of kaolin clay on intumescent fire retardant coating composition for fire protection of structural steel substrate. *Polymer Degradation and Stability*, 110: 91-103. <https://doi.org/10.1016/j.polymdegradstab.2014.08.017>
- [22] Ullah, S., Ahmad, F., Yusoff, P.M. (2013). Effect of boric acid and melamine on the intumescent fire-retardant coating composition for the fire protection of structural steel substrates. *Journal of Applied Polymer Science*, 128(5): 2983-2993. <https://doi.org/10.1002/app.38318>
- [23] Wang, G., Yang, J. (2011). Influences of glass flakes on fire protection and water resistance of waterborne intumescent fire resistive coating for steel structure. *Progress in Organic Coatings*, 70(2-3): 150-156.

<https://doi.org/10.1016/j.porgcoat.2010.10.007>

- [24] Weisheim, W., Schaumann, P., Sander, L., Zehfuß, J. (2019). Numerical model for the fire protection performance and the design of intumescent coatings on structural steel exposed to natural fires. *Journal of Structural Fire Engineering*, 11(1): 33-50. <https://doi.org/10.1108/JSFE-01-2019-0004>
- [25] Alam, N., Nadjai, A., Charlier, M., Vassart, O., Welch, S., Sjöström, J., Dai, X. (2022). Large scale travelling fire tests with open ventilation conditions and their effect on the surrounding steel structure—The second fire test. *Journal of Constructional Steel Research*, 188: 107032. <https://doi.org/10.1016/j.jcsr.2021.107032>
- [26] Hou, J.H., Li, H.M., Xie, D., Qian, L.L., Tang, B.J. (2022). Fire resistance analysis of prestressed steel structure based on the study of high temperature mechanical properties of steel strands. *Advances in Transdisciplinary Engineering*, 20: 990-995.
- [27] Manco, M.R., Vaz, M.A., Cyrino, J.C., Landesmann, A. (2021). Thermomechanical performance of offshore topside steel structure exposed to localised fire conditions. *Marine Structures*, 76: 102924. <https://doi.org/10.1016/j.marstruc.2020.102924>
- [28] Suwondo, R., Cunningham, L., Gillie, M., Bailey, C. (2021). Analysis of the robustness of a steel frame structure with composite floors subject to multiple fire scenarios. *Advances in Structural Engineering*, 24(10): 2076-2089. <https://doi.org/10.1177/1369433221992494>